Journal of Microbiology (2020) Vol. 58, No. 7, pp. 606–613
DOI 10.1007/s12275-020-0089-1

eISSN 1976-3794
pISSN 1225-8873

Structural and sequence comparisons of bacterial enoyl-CoA isomerase and enoyl-CoA hydratase[§]

Jisub Hwang[1,2†], Chang-Sook Jeong[1,2†], Chang Woo Lee[1†], Seung Chul Shin[3], Han-Woo Kim[1,2], Sung Gu Lee[1,2], Ui Joung Youn[2,3], Chang Sup Lee[4], Tae-Jin Oh[5,6,7], Hak Jun Kim[8], Hyun Park[9*], Hyun Ho Park[10*], and Jun Hyuck Lee[1,2*]

[1]*Unit of Research for Practical Application, Korea Polar Research Institute, Incheon 21990, Republic of Korea*
[2]*Department of Polar Sciences, University of Science and Technology, Incheon 21990, Republic of Korea*
[3]*Division of Life Sciences, Korea Polar Research Institute, Incheon 21990, Republic of Korea*
[4]*College of Pharmacy and Research Institute of Pharmaceutical Sciences, Gyeongsang National University, Jinju 52828, Republic of Korea*
[5]*Department of Life Science and Biochemical Engineering, Graduate School, SunMoon University, Asan 31460, Republic of Korea*
[6]*Genome-based BioIT Convergence Institute, Asan 31460, Republic of Korea*
[7]*Department of Pharmaceutical Engineering and Biotechnology, SunMoon University, Asan 31460, Republic of Korea*
[8]*Department of Chemistry, Pukyong National University, Busan 48513, Republic of Korea*
[9]*Division of Biotechnology, College of Life Sciences and Biotechnology, Korea University, Seoul 02841, Republic of Korea*
[10]*College of Pharmacy, Chung-Ang University, Seoul 06974, Republic of Korea*

(Received Feb 18, 2020 / Revised Mar 30, 2020 / Accepted Mar 30, 2020)

Crystal structures of enoyl-coenzyme A (CoA) isomerase from *Bosea* sp. PAMC 26642 (*Bo*ECI) and enoyl-CoA hydratase from *Hymenobacter* sp. PAMC 26628 (*Hy*ECH) were determined at 2.35 and 2.70 Å resolution, respectively. *Bo*ECI and *Hy*ECH are members of the crotonase superfamily and are enzymes known to be involved in fatty acid degradation. Structurally, these enzymes are highly similar except for the orientation of their C-terminal helix domain. Analytical ultracentrifugation was performed to determine the oligomerization states of *Bo*ECI and *Hy*ECH revealing they exist as trimers in solution. However, their putative ligand-binding sites and active site residue compositions are dissimilar. Comparative sequence and structural analysis revealed that the active site of *Bo*ECI had one glutamate residue (Glu135), this site is occupied by an aspartate in some ECIs, and the active sites of *Hy*ECH had two highly conserved glutamate residues (Glu118 and Glu138). Moreover, *Hy*ECH possesses a salt bridge interaction between Glu98 and Arg152 near the active site. This interaction may allow the catalytic Glu118 residue to have a specific conformation for the ECH enzyme reaction. This salt bridge interaction is highly conserved in known bacterial ECH structures and ECI enzymes do not have this type of interaction. Collectively, our comparative sequential and structural studies have provided useful information to distinguish and classify two similar bacterial crotonase superfamily enzymes.

Keywords: crystal structure, enoyl-CoA isomerase, enoyl-CoA hydratase, X-ray crystallography

Introduction

Crotonase family enzymes catalyze carbon-carbon bond isomerization and the hydrolysis of thioesters from acyl substrates covalently linked to coenzyme A (CoA) via a thioester bond (Hamed *et al.*, 2008). Thus, the crotonase family enzymes are also called enoyl-CoA hydratase/isomerase family proteins and they are involved in the degradation or biosynthesis of various enoyl group compounds and fatty acids in all organisms (Holden *et al.*, 2001; Zhang *et al.*, 2002; van Weeghel *et al.*, 2012).

Enoyl-CoA isomerase (ECI) catalyzes the conversion of the double bond in acyl chains of enoyl-CoA substrates. ECI has one catalytic acid residue (Glu or Asp) providing the proton to change the double bond position of the enoyl-CoA substrate. During this reaction, the thioester oxygen atom bonds to the oxyanion hole (Muller-Newen *et al.*, 1995; Mursula *et al.*, 2004; Partanen *et al.*, 2004; Hubbard *et al.*, 2005; Onwukwe *et al.*, 2015; Srivastava *et al.*, 2015). Whereas, enoyl-CoA hydratase (ECH) contains two glutamate residues that act as a catalytic acid and base for thioester bond hydrolysis and facilitates the addition of a water molecule across the double bond of an enoyl-CoA substrate, resulting in the formation of a hydroxyl enoyl-CoA product (Hofstein *et al.*, 1999; Kiema *et al.*, 1999; Bahnson *et al.*, 2002; Agnihotri and Liu, 2003). Although these two enzymes have low sequence similarity, they share a similar three-dimensional structure as well as oligomerization state (trimer or dimer of trimer) (Mursula *et al.*, 2004; Partanen *et al.*, 2004; Hubbard *et al.*, 2005).

Several bacterial ECI and ECH structures have been reported. In Kichise *et al.* (2009) determined the crystal structure of PaaG from *Thermus thermophilus* HB8. PaaG is a member of the crotonase superfamily and is involved in the degradation of phenylacetic acid and the Asp136 residue

[†]These authors contributed equally to this work.
*For correspondence. (H. Park) E-mail: hpark@korea.ac.kr; Tel.: +82-2-3290-3051 / (H.H. Park) E-mail: xrayleox@cau.ac.kr; Tel.: +82-2-820-5930; Fax: +82-2-820-5933 / (J.H. Lee) E-mail: junhyucklee@kopri.re.kr; Tel.: +82-32-760-5555; Fax: +82-32-760-5509
[§]Supplemental material for this article may be found at http://www.springerlink.com/content/120956

may be the single active site residue (Kichise *et al.*, 2009). In Srivastava *et al.* (2015) identified two crystal structures of cis-trans ECIs from *Mycobacterium tuberculosis* (Mtb) and tried to classify 21 Mtb homologs into ECH, ECI, or bifunctional enzymes using the position of catalytic Glu and Asp residues in multiple sequence alignment. The crystal structure of 3-hydroxypropionyl-CoA dehydratase (*Ms*3HPCD) from *Metallosphaera sedula* shows that *Ms*3HPCD contains a smaller substrate-binding cavity than other ECHs because of a3 helix movement and bulky aromatic residues (Lee and Kim, 2018). Crotonase from *Clostridium acetobutylicum* (*Ca*CRT) catalyzes the dehydration of 3-hydroxybutyryl-CoA to crotonyl-CoA. The crystal structure of *Ca*CRT revealed that two phenylalanine residues (Phe143 and Phe233) are important for substrate specificity and substrate binding (Kim *et al.*, 2014). In Tan *et al.* (2013) identified the crystal structure of DmdD from *Ruegeria pomeroyi*. Structural information together with site-directed mutagenesis and activity assay results suggested that the two glutamate residues (Glu121 and Glu141) are catalytic residues for the hydrolysis of methylthioacryloyl-CoA by DmdD (Tan *et al.*, 2013). In Bock *et al.* (2016) published the structure of LiuC (3-hydroxy-3-methylglutaconyl CoA dehydratase) from *Myxococcus xanthus*. Structure analysis and substrate binding model studies revealed that Glu112 and Glu132 residues are important for the acid-base reaction mechanism of LiuC (Bock *et al.*, 2016). Numerous ECI and ECH enzymes have been identified; however, the structural and functional discrimination of these two enzyme groups is still unclear.

We report on two crystal structures of ECI from *Bosea* sp. PAMC 26642 (*Bo*ECI) and ECH from *Hymenobacter* sp. PAMC 26628 (*Hy*ECH) and make structural and sequence comparisons between these and other crotonase family enzymes revealing the distinct characteristics of bacterial ECI and ECH groups. ECH enzyme groups have a unique α5-α6 loop and a salt bridge near their active site that is thought to be important for catalytic reactions of ECH enzymes. Our findings provide useful information for classifying newly identified bacterial ECI and ECH proteins.

Materials and Methods

Sequence analysis and comparison of *Bo*ECI and *Hy*ECH

The ECI from *Bosea* sp. (PAMC 26642) encodes a protein of 245 amino acids with an overall guanine + cytosine (G + C) content of 67.1%. Whereas, the ECH from *Hymenobacter* sp. (PAMC 26628) encodes a protein of 263 amino acids with an overall G + C content of 67.7%. Both sequences were compared with bacteria/yeast ECI and ECH groups including sequences of monofunctional ECI obtained from *Mycolicibacterium smegmatis* (PDB code 5E0N; UniProtKB code A0QX16), Δ(3)-Δ(2)-ECI obtained from *Saccharomyces cerevisiae* (PDB code 1HNU; UniProtKB code Q05871), phenylacetic acid degradation protein PaaG from *T. thermophiles* (PDB code 3HRX; UniProtKB code Q5SLK3) 4-chlorobenzoyl-CoA dehalogenase obtained from *Pseudomonas* sp. (strain CBS-3) (PDB code 1NZY; UniProtKB code A5JTM5), 3-hydroxypropionyl-CoA dehydratase from *M. sedular* (PDB code 5ZAI; UniProtKB code A4YI89), crotonase obtained from *C. acetobutylicum* (PDB code 5Z7R; UniProtKB code P52046), ECH from *Bacillus anthracis* (PDB code 3KQF; UniProtKB code A0A0F7RDV5), 3-hydroxy-3-methylglutaconyl-CoA dehydratase obtained from *M. xanthus* (PDB code 5JBW; UniProtKB code Q1D5Y4), and crotonase superfamily enzyme obtained from *R. pomeroyi* (PDB code 4IZB; UniProtKB code Q5LLW6). Multiple sequence alignment was performed with *Clustal X* as previously described by Thompson *et al.* (2002) and edited using *Espript* 3.0 as previously described by Robert and Gouet (2014).

Cloning, expression, and purification of *Bo*ECI and *Hy*ECH

The ECI and ECH coding gene in *Bosea* sp. (PAMC 26642) and *Hymenobacter* sp. (PAMC 26628) were used as a template for PCR. The amplified DNA fragments were cloned into the pET-28a expression vector using *Nde*I and *Xho*I restriction enzymes with a 6xHis-tag and thrombin protease recognition site (Bioneer). After confirmation by DNA sequencing, the resulting plasmid was transformed into *Escherichia coli* strain BL21 (DE3) cells for protein expression. The cells were grown in 2 L of Luria-Bertani (LB) medium containing kanamycin (50 μg/ml) at 37°C. When the optical density at 600 nm (OD_{600}) reached 0.8, overnight expression was induced with 0.5 mM isopropyl-1-thio-β-D-galactopyranoside (IPTG) at 25°C. The cells were collected by centrifugation at 6,000 rpm, 4°C for 30 min and then resuspended in cell lysis buffer (50 mM sodium phosphate, 300 mM NaCl, 5 mM imidazole, pH 8.0). After sonication on ice and centrifugation at 15,000 rpm, 4°C for 1 h, the collected supernatant was allowed to flow into a pre-equilibrated Ni-NTA column (Qiagen). The unbound proteins flowed through and the polyhistidine-tagged proteins bound to the Ni-NTA resin were washed with wash buffer (50 mM sodium phosphate, 300 mM NaCl, 30 mM imidazole, pH 8.0). The proteins were then eluted with elution buffer (50 mM sodium phosphate, 300 mM NaCl, 300 mM imidazole, pH 8.0). The fractions of targeted polyhistidine-tagged proteins were collected and then concentrated to 5 ml using Amicon Ultra Centrifugal Filter (Ultracel-10K; Millipore). The poly-histidine tag was cleaved by thrombin treatment for 48 h at 4°C with inversion. The precipitates were removed by centrifugation and then the cleaved protein solution was loaded onto a Superdex 200 column (GE Healthcare) pre-equilibrated with 50 mM sodium phosphate, 300 mM NaCl (pH 8.0). The fractions of *Bo*ECI and *Hy*ECH proteins were collected and concentrated to 64 and 67 mg/ml, respectively, using Amicon Ultra Centrifugal Filters.

Crystallization and data collection

Wild-type *Bo*ECI and *Hy*ECH crystallization were performed using a commercially available solution kit, MCSG I-IV (Molecular Dimensions), Index, SaltRx (Hampton Research) using the sitting-drop vapor-diffusion method at 23°C in 96-well crystallization plates (Molecular Dimensions). The aliquots of screening solution and protein samples were performed using a mosquito crystallization robot (TTP Labtech). A 300 nl volume of two different concentrated protein solutions was mixed with a 300 nl reservoir solution and equilibrated against a 70 μl reservoir solution. Among some of

Table 1. X-ray diffraction data collection and refinement statistics

Data set	*Bo*ECI	*Hy*ECH
X-ray source	BL-5C	BL-5C
Space group	$I2_3$	$P4_22_12$
Unit-cell parameters (Å, °)	a, b, c = 114.5 α, β, γ = 90.0°	a, b = 128.3, c = 103.0 α, β, γ = 90.0°
Wavelength (Å)	1.00	0.97942
Resolution (Å)	50.00–2.35 (2.39–2.35)	50.00–2.70 (2.75–2.70)
Total reflections	345677	354664
Unique reflections	10379 (521)	45738 (1203)
Average I/σ (I)	69.8	49.7
R_{merge}[a]	0.123 (0.708)	0.092 (0.508)
Redundancy	33.3 (29.5)	14.5 (13.9)
Completeness (%)	99.9 (100)	100 (100)
Refinement		
Resolution range (Å)	46.8–2.36 (2.43–2.36)	40.6–2.69 (2.76–2.69)
No. of reflections of working set	10376 (2436)	24490 (2469)
No. of reflections of test set	502 (135)	1219 (153)
No. of amino acid residues	237	789
No. of water molecules	39	18
R_{cryst}[b]	0.212 (0.206)	0.188 (0.212)
R_{free}[c]	0.277 (0.327)	0.237 (0.302)
R.m.s. bond length (Å)	0.009	0.008
R.m.s. bond angle (°)	0.941	0.980
Average B value (Å^2) (protein)	44.2	56.9
Average B value (Å^2) (solvent)	44.5	43.7

[a] $R_{merge} = \Sigma \mid <I> - I \mid / \Sigma <I>$.
[b] $R_{cryst} = \Sigma \mid |Fo| - |Fc| \mid / \Sigma |Fo|$.
[c] R_{free} calculated with 5% of all reflections excluded from refinement stages using high-resolution data
Values in parentheses refer to the highest resolution shells

the crystals, the most optimally shaped *Bo*ECI crystals were observed in 2 days with 33 mg/ml concentrated *Bo*ECI and a reservoir solution composed of 0.2 M zinc acetate, 0.1 M imidazole (pH 8.0), 20% (v/v) 1,4-butanediol (MCSG III #H6) at 23°C. The *Hy*ECH crystals were visible under several screening conditions and the most optimal shaped crystals were observed in 3 days with 35 mg/ml concentrated *Hy*ECH solution and a reservoir solution composed of 0.16 M magnesium acetate, 0.08 M sodium cacodylate (pH 6.5), 16% (w/v) polyethylene glycol (PEG) 8000 and 20% (v/v) glycerol (MCSG III #C5) at 23°C. The single crystals of *Bo*ECI and *Hy*ECH were mounted with a cryoloop and protected from the liquid nitrogen gas stream using 30% (v/v) glycerol containing optimal screening solution and Paratone-N oil (Hampton Research), respectively. X-ray diffraction data for *Bo*ECI and *Hy*ECH containing 300 and 360 images, respectively, were collected at the BL-5C beamline in the Pohang Accelerator Laboratory (PAL) (Park *et al.*, 2017) with an oscillation range of 1° per image with 1 sec exposure using the CCD EIGER 9M detector (Dectris). The data were indexed, integrated, and scaled using the *HKL*-2000 (Otwinowski and Minor, 1997; Table 1).

Structural determination and refinement

The crystal structures of *Bo*ECI and *Hy*ECH were determined by molecular replacement using *MORLEP* (Vagin and Teplyakov, 2010). Putative enoyl-CoA hydratase/isomerase from *A. baumannii* (PDB code 3FDU) with 41% sequence identity and 3-hydroxypropionyl-CoA dehydratase from *M. sedula* (PDB code 5ZAI) with 47% sequence identity were used as template models for *Bo*ECI and *Hy*ECH, respectively. The *Bo*ECI crystal volume per unit molecular weight (V_M) was approximately 2.50 Å^3/Da with a solvent content of 50.85% by volume when the asymmetric unit was assumed to contain one *Bo*ECI molecule. Whereas the *Hy*ECH crystal volume per unit molecular weight (V_M) was about 2.62 Å^3/Da with a solvent content of 53.01% by volume when the asymmetric unit was assumed to contain three *Hy*ECH molecules (Matthews, 1968; Kantardjieff and Rupp, 2003). Manual model building and refinement were performed by *WinCoot* (Emsley and Cowtan, 2004) and *Refmac5* from the *CCP4i* suite (Murshudov *et al.*, 2011). Water molecules were added and then the overall structures were refined by *Phenix* (Afonine *et al.*, 2012). The final model of *Bo*ECI had a R_{cryst} value of 21.2% and a R_{free} value of 27.7% with a total of 238 amino acid residues and 39 water molecules. The final model of *Hy*ECH had a R_{cryst} value of 18.8% and a R_{free} value of 23.7% with a total of 789 amino acid residues and 18 water molecules. The final refined model and reflection data of *Bo*ECI and *Hy*ECH are deposited in Protein Data Bank with PDB codes of 6LVO and 6LVP, respectively. PyMol was used to visualize and produce figures (Delano, 2002).

Results and Discussion

Overall structures of *Bo*ECI and *Hy*ECH

The crystal structures of ECI obtained from *Bosea* sp. PAMC 26642 (*Bo*ECI) and ECH obtained from *Hymenobacter* sp. PAMC 26628 (*Hy*ECH) were determined at 2.35 Å and 2.70 Å resolution, respectively (Fig. 1A and B). The molecular replacement method was used to determine the structures of both *Bo*ECI and *Hy*ECH by using the crystal structures of enoyl-CoA hydratase/isomerase from *Acinetobacter baumannii* (PDB code 3FDU) and 3-hydroxypropionyl-CoA dehydratase from *M. sedula* (PDB code 5AZI) as template models, respectively. The overall structures of *Bo*ECI and *Hy*ECH are similar to those of the enoyl-CoA hydratase/isomerase group of the crotonase superfamily. The two enzymes show a ββα fold on the N-domain (residues 3 to 130 in *Bo*ECI and residues 8 to 141 in *Hy*ECH), referred to as the crotonase fold, which is a canonical secondary structure of the crotonase superfamily (Hamed *et al.*, 2008). First, the overall structure of *Bo*ECI consists of ten α-helices and two β-sheets formed by five mixed β-strands and two parallel β-strands. The electron density of the residues from Phe68 to Thr74 was poorly defined. Therefore, these regions have not been modeled in the final structure of *Bo*ECI. Second, the overall structure of *Hy*ECH consists of twelve α-helices and one β-sheet including six mixed β-strands. Unlike the *Bo*ECI structure, all residues can be modeled and included in the final structure of *Hy*ECH.

Results of the structural homolog search using the DALI server (Holm, 2019) showed that many crotonase superfamily proteins share structural similarities with *Bo*ECI and *Hy*ECH. The crystal structure of enoyl-CoA hydratase/isomerase from *A. baumannii* (PDB code 3FDU) is the most

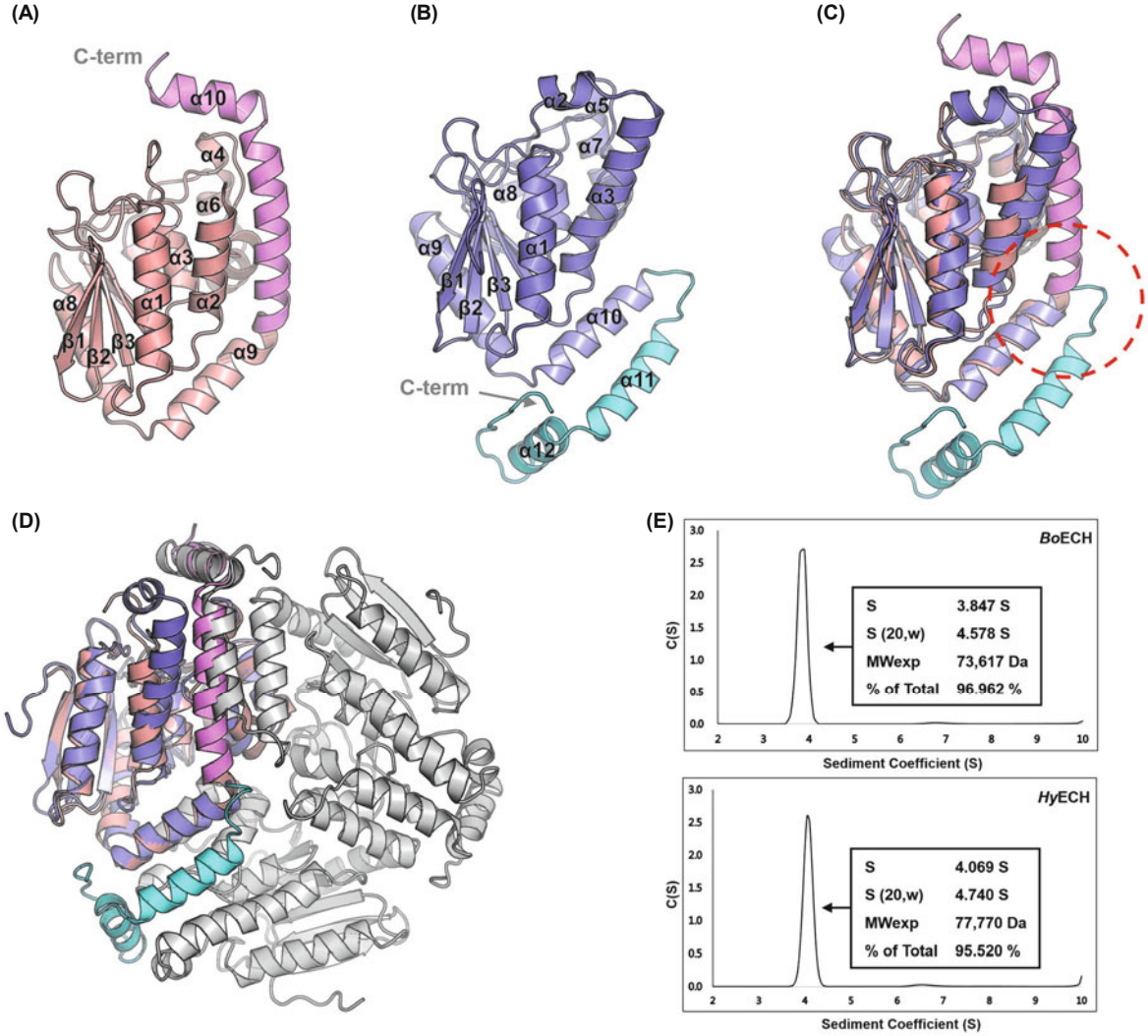

Fig. 1. The structure of *Bo*ECI and *Hy*ECH. (A) The monomer structure of *Bo*ECI with the C-terminal helix region (residues 211–245) marked in violet. (B) The monomer structure of *Hy*ECH with the C-terminal helix region (residues 223–263) marked in cyan. (C) The monomeric structure of *Bo*ECI superimposed on *Hy*ECH demonstrating the remarkable difference in the orientation of the C-terminal helix region between the two structures. (D) Trimeric *Bo*ECI superimposed on *Hy*ECH. (E) Analytical ultracentrifugation profiles of *Bo*ECI and *Hy*ECI indicating they are trimeric in solution. *Bo*ECI, enoyl-CoA isomerase from *Bosea* sp. PAMC 26642; *Hy*ECH, enoyl-CoA hydratase from *Hymenobacter* sp. PAMC 26628.

similar to *Bo*ECI and the crystal structure of 3-hydroxypropionyl-CoA dehydratase from *M. sedula* (PDB code 5AZI) is the most similar to *Hy*ECH (Supplementary data Tables S1 and S2). Structural superposition between *Bo*ECI and *Hy*ECH shows high similarities with the 1.33 Å r.m.s deviation over 176 C_α atoms (Fig. 1C). However, intuitive structural differences were observed in the C-terminal helix region (residues 211 to 245 in *Bo*ECI and residues 223 to 263 in *Hy*ECH). The α9 helix of *Bo*ECI was stretched straight out and formed a long α-helix but the corresponding region of *Hy*ECH was bent by approximately 180°, stretching in the opposite direction. However, the differences in the C-terminal helix region are structurally complementary in the trimer state, wherein the structures of both the trimers are highly similar with the 1.53 Å r.m.s deviation over 271 C_α atoms (Fig. 1D). Analytical ultracentrifugation confirmed *Bo*ECI and *Hy*ECH are trimers in solution (Fig. 1E) (Schuck, 2000). In addition, the C-terminal helix is located near the putative ligand-binding pocket. In the *Hy*ECH structure, the C-terminal helix is involved in forming the ligand-binding site with other subunits. Therefore, the composition of residues in the C-terminal helix region is expected to affect the ligand-binding mode.

Active site differences between *Bo*ECI and *Hy*ECH

The result of multiple sequence alignment with bacterial/yeast enoyl-CoA hydratase/isomerase family enzymes indicated that the ECI and ECH groups have conserved catalytic residues; two glutamates in ECH and one glutamate or aspartate in ECI, respectively (Fig. 2). Likewise, *Bo*ECI and *Hy*ECH also contain conserved catalytic residues at the corresponding site. The overall structures of *Bo*ECI and *Hy*ECH display significant similarity; however, the compositions of their putative ligand-binding pocket and active site residues are different. In both the structures, the putative ligand-binding pockets consist of α-helices located in the outer edge of the trimer structure; α1, α2, α3, α4, α9, and α10 in *Bo*ECI and α2, α3, α4, α5, α6, α11, and α12 in *Hy*ECH. The outer surface, near the substrate-binding site on both structures, may be positively charged to attract negatively charged ligands (Fig. 3A and D). In the *Bo*ECI structure, the conserved catalytic residue of Glu135 is located in the α4-α5 loop region

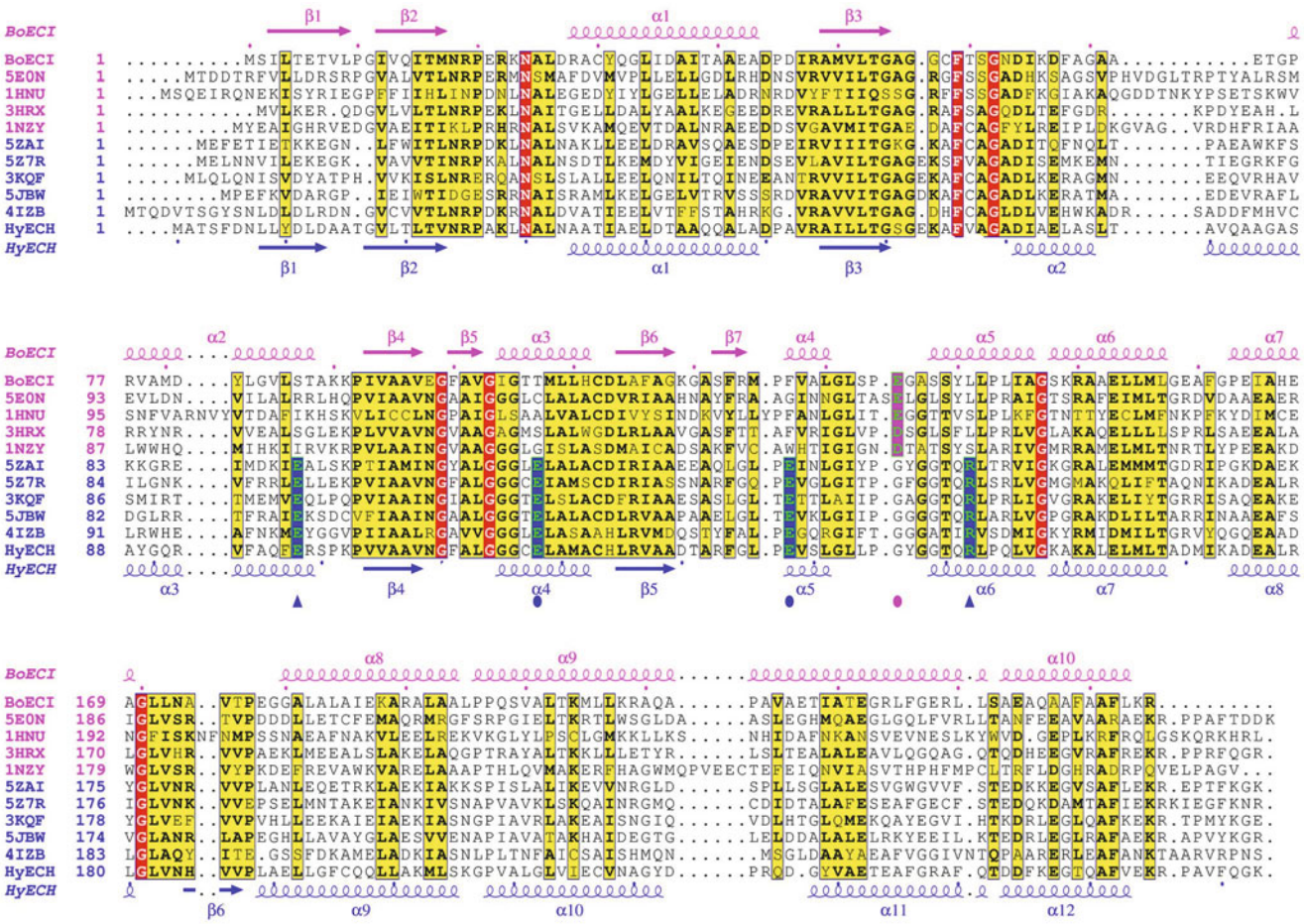

Fig. 2. Multiple sequence alignment of *Bo*ECI and *Hy*ECH with bacteria/yeast ECI and ECH groups. The secondary structural elements of *Bo*ECI and *Hy*ECH are shown on the top and bottom lines of each sequence alignment, respectively. The highly conserved catalytic residue Glu135 of *Bo*ECI is marked with a pink circle in the ECI group. The two strictly conserved glutamic acid residues Glu118 and Glu138 of *Hy*ECH are marked with blue circles in the ECH group. Residues Glu98 and Arg152 participating in the salt bridge interaction of *Hy*ECH are indicated by blue triangles. *Bo*ECI, enoyl-CoA isomerase from *Bosea* sp. PAMC 26642; *Hy*ECH, enoyl-CoA hydratase from *Hymenobacter* sp. PAMC 26628; ECI, enoyl-CoA isomerase; ECH, enoyl-CoA hydratase.

(Fig. 3B). The catalytic residue of Glu135 interacts with the main chain amide group of Ile104 and the side chain of Thr-107 that are located in the α3 helix. Several hydrophobic residues (Ile65, Pro76, Ala79, Leu83, Ile104, Phe127, Leu130, Leu132, Phe 226, Leu230, Phe239, and Phe242) form a long channel pocket for ligand binding in *Bo*ECI. It is considered that the flexible and disordered region (residues 68 to 74) of the β3-α2 loop may act as a cap for substrate entry and product release in *Bo*ECI. This cap exists in many different forms in other ECI structures. In the structure of PaaG from *T. thermophilus* (PDB code 3HRX), this corresponding loop region is extended straight from the α2 helix. The ECI structure of the protein obtained from *Pseudoalteromonas atlantica* (PDB code 5VE2), forms an additional α-helix rather than a loop in this region and covers the putative ligand-binding pocket (Fig. 3C). These regions have a higher relative average B-factor (53.2 $Å^2$) than other regions. Various structural modes and the high B-factor of the corresponding region may explain the intrinsic flexibility of the loop region (residues 55 to 75) in *Bo*ECI. In the structure of *Hy*ECH, the catalytic residues of Glu118 and Glu138 are located in the α4 and α5-helices, respectively (Fig. 3E). Glu118 interacts with the main chain amide groups that are located in the α5-α6 loop region. The putative ligand-binding pocket is composed of Leu32, Ile37, Ala70, Ile72, Glu74, Leu75, Leu78, Ala86, Pro137, Leu144, and Tyr147. Furthermore, the residues (Phe236, Phe240, Phe245, and Phe252) from the other subunit also participate in forming the ligand-binding pocket of *Hy*ECH.

Structures of the cap region (residues 61 to 86 in *Hy*ECH) in ECHs showed a higher relative average B-factor (56.9 $Å^2$) compared to other regions. The cap region of 3-hydroxypropionyl-CoA dehydratase obtained from *M. sedula* (3HPCD, PDB code 5ZAI) forms a small α-helix above the catalytic residues. The ECH from *M. tuberculosis* (*Mt*ECH, PDB code 3H81) has also the small α-helix in the capping region. In the *Mt*ECH structure, the long α3-helix is divided into two α-helices (Fig. 3F). This separated α3-helix is also observed in other ECH structures such as crotonase obtained from *M. tuberculosis* (PDB code 3Q0G) and ECH obtained from *Roseovarius nubinhibens* (PDB code 5XZD). Thus, it is suspected that this α3-helix rearrangement may affect and change the cavity size of the substrate-binding region in ECHs.

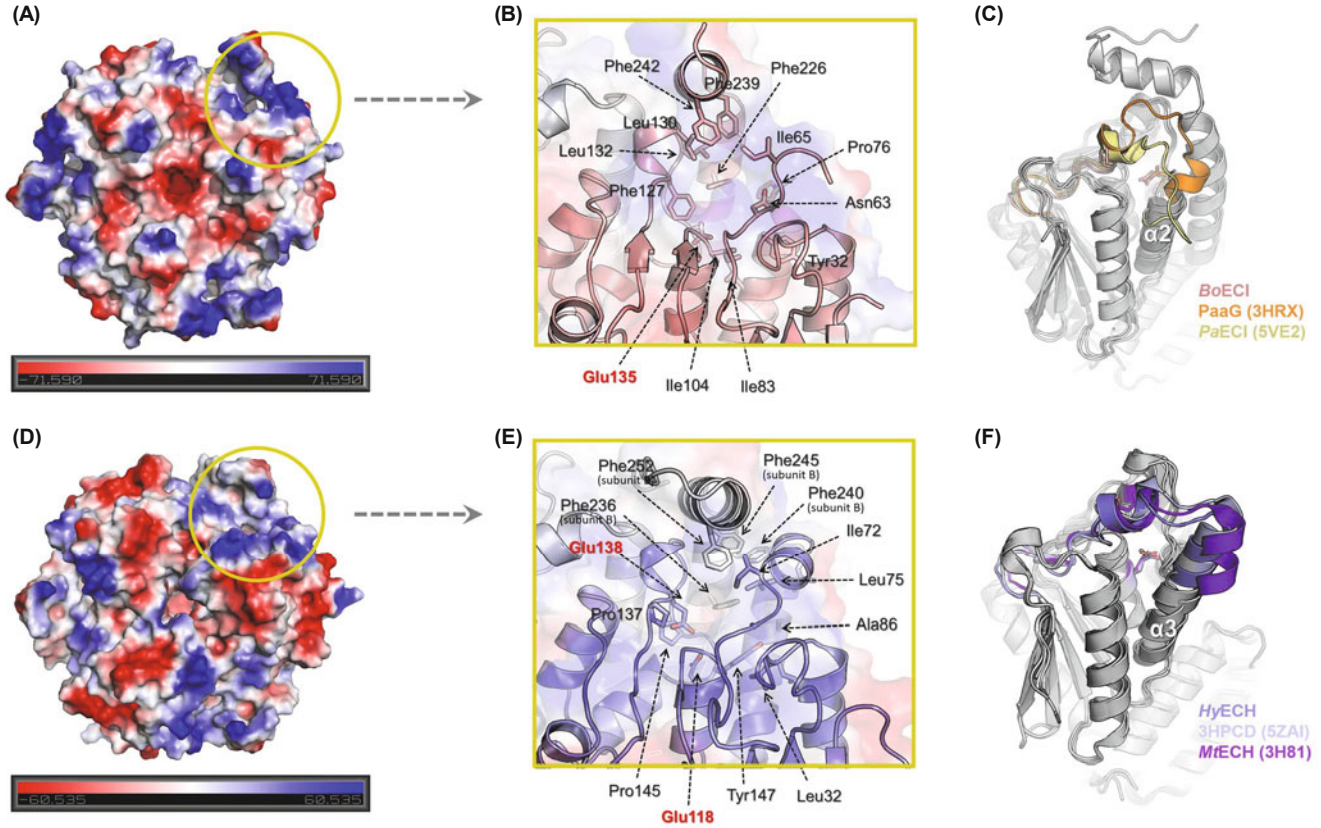

Fig. 3. The active sites of *Bo*ECI and *Hy*ECH. (A) The electrostatic surface potential of the trimeric *Bo*ECI structure shows that the periphery of the putative ligand-binding site has a positive charge. (B) Close-up view of the putative ligand-binding site of *Bo*ECI. The residues that are located in the putative ligand-binding site are shown as a stick model and colored in pinkish-orange. (C) Structural superposition of ECIs. Capping loop regions of *Bo*ECI, PaaG (PDB code 3HRX), and *Pa*ECI (5VE2) are colored in pinkish-orange, orange, and pale yellow, respectively. (D) The electrostatic surface potential of the trimeric *Hy*ECH structure also shows that the periphery of the putative ligand-binding site has a positive charge. (E) Close-up view of the putative ligand-binding site of *Hy*ECH. The residues that are located in the putative ligand-binding site are shown by the stick model. The subunit A residues are colored in slate and subunit B residues are colored in gray. (F) Structural superposition of ECHs. Cap regions of *Hy*ECH, 3HPCD (PDB code 5ZAI), and *Mt*ECH (PDB code 3H81) are colored in slate, light blue, and purplish-blue, respectively. *Bo*ECI, enoyl-CoA isomerase from *Bosea* sp. PAMC 26642; *Hy*ECH, enoyl-CoA hydratase from *Hymenobacter* sp. PAMC 26628; ECI, enoyl-CoA isomerase; ECH, enoyl-CoA hydratase. *Mt*ECH, ECH from *M. tuberculosis* (PDB code 3H81).

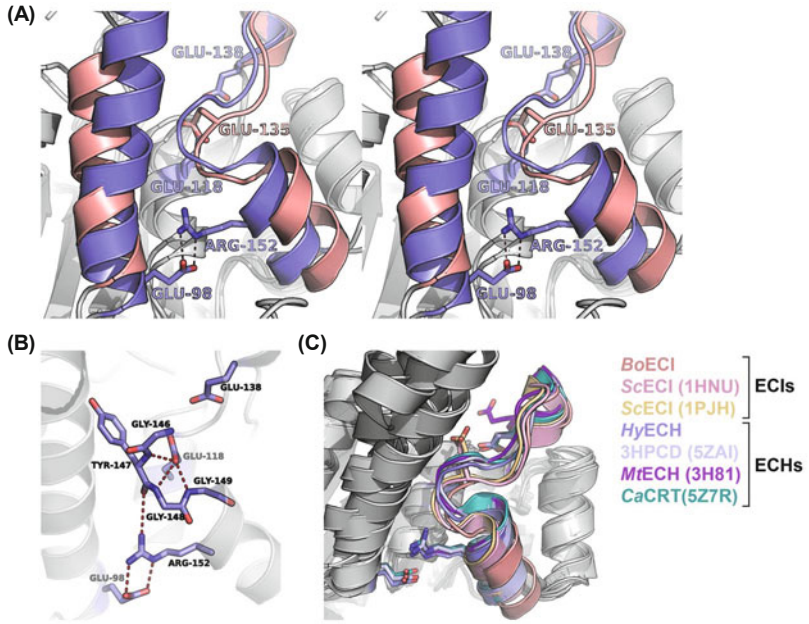

Fig. 4. Structural comparison between *Bo*ECI and *Hy*ECH. (A) Stereo view of the superimposed structures of *Bo*ECI and *Hy*ECH shows that the salt bridge between Glu98 and Arg152 is the key interaction for distinguishing between ECHs. (B) Specific interactions including salt bridge interaction between Glu98 and Arg152 in the active site of *Hy*ECH are shown by the stick model. The salt bridge interaction between Glu98 and Arg152 is important for the catalytic residue configuration in *Hy*ECH. (C) The salt bridge interaction between Glu98 and Arg152 found in *Hy*ECH is highly conserved in all bacterial ECH structures but the ECI groups do not have this type of interaction. *Bo*ECI, enoyl-CoA isomerase from *Bosea* sp. PAMC 26642; *Hy*ECH, enoyl-CoA hydratase from *Hymenobacter* sp. PAMC 26628; ECI, enoyl-CoA isomerase; ECH, enoyl-CoA hydratase.

Sequential and structural comparison between *Bo*ECI and *Hy*ECH

Another structural difference was observed near the active site, except the composition of catalytic residues. In *Hy*ECH, the salt bridge interaction between α3 and α6 helices increases the proximity between both these helices compared to their proximity in *Bo*ECI (Fig. 4A). These two α-helices contain the necessary residues for substrate binding in both enzymes. In detail, the Arg152 residue from the α6-helix region tightly interacts with the Glu98 residue from the α3-helix region. Furthermore, Arg152 interacts with the main chain O atom of Tyr147. This interaction may affect serial conformation changes and contribute to the structural differences in the active sites of *Hy*ECH and *Bo*ECI. As a result, the α5-α6 loop region (residues Gly142 to Gly148) of *Hy*ECH turns inward, and the catalytic residue of Glu118 is allowed to interact with the main chain amide groups of Tyr147, Gly148, and Gly149 located in the α5-α6 loop region (Fig. 4B). Interestingly, this specific salt bridge interaction (Glu98 to Arg152 in *Hy*ECH) and the structural feature of the inward α5-α6 loop were identified only in ECHs. Structural alignments using known bacterial homologs of ECIs and ECHs clearly show that ECHs have an inward α5-α6 loop region in the substrate-binding site (Fig. 4C). A multiple sequence alignment confirmed that the Glu and Arg residues that formed the salt bridge are highly conserved in ECHs but not ECIs (Fig. 2). Furthermore, when the *Hy*ECH sequence was compared against the non-redundant GenBank database using Basic Local Alignment Search Tool (BLAST) salt bridge making residues were found in novel ECH enzymes from other microbial sources (Supplementary data Fig. S1).

In conclusion, our multiple sequence alignment and comparative structural analysis of *Bo*ECI, *Hy*ECH, and their homologs revealed clear structural differences between ECI and ECH, including the flexible cap region in *Bo*ECI and the unique salt bridge interaction that exists only in the ECH group of enzymes. These findings may be useful for characterizing the functional differences between ECI and ECH in addition to their usefulness in classifying the bacterial crotonase superfamily enzymes as ECI or ECH.

Acknowledgments

We would like to thank the staff at the X-ray core facility of Korea Basic Science Institute (KBSI) (Ochang, Korea) and BL-5C of the Pohang Accelerator Laboratory (Pohang, Korea) for their kind help in data collection. This work was supported by the Korea Polar Research Institute (KOPRI; grant numbers PE19210 and PE20040). This research was also supported by a National Research Foundation of Korea Grant from the Korean Government (MSIT; the Ministry of Science and ICT) (NRF-2017M1A5A1013568) (KOPRI-PN20082) (Title: Circum Arctic Permafrost Environment Change Monitoring, Future Prediction and development Techniques of useful biomaterials [CAPEC Project]).

References

Afonine, P.V., Grosse-Kunstleve, R.W., Echols, N., Headd, J.J., Moriarty, N.W., Mustyakimov, M., Terwilliger, T.C., Urzhumtsev, A., Zwart, P.H., and Adams, P.D. 2012. Towards automated crystallographic structure refinement with *phenix.refine*. *Acta Crystallogr. D Biol. Crystallogr*. **68**, 352–367.

Agnihotri, G. and Liu, H.W. 2003. Enoyl-CoA hydratase: reaction, mechanism, and inhibition. *Bioorg. Med. Chem*. **11**, 9–20.

Bahnson, B.J., Anderson, V.E., and Petsko, G.A. 2002. Structural mechanism of enoyl-CoA hydratase: three atoms from a single water are added in either an E1cb stepwise or concerted fashion. *Biochemistry* **41**, 2621–2629.

Bock, T., Reichelt, J., Muller, R., and Blankenfeldt, W. 2016. The structure of LiuC, a 3-hydroxy-3-methylglutaconyl CoA dehydratase involved in isovaleryl-CoA biosynthesis in *Myxococcus*

xanthus, reveals insights into specificity and catalysis. *Chembiochem* **17**, 1658–1664.

Delano, W.L. 2002. The PyMOL molecular graphics system. http://www.pymol.org.

Emsley, P. and Cowtan, K. 2004. Coot: model-building tools for molecular graphics. *Acta Crystallogr. D Biol. Crystallogr*. **60**, 2126–2132.

Hamed, R.B., Batchelar, E.T., Clifton, I.J., and Schofield, C.J. 2008. Mechanisms and structures of crotonase superfamily enzymes – how nature controls enolate and oxyanion reactivity. *Cell. Mol. Life Sci*. **65**, 2507–2527.

Hofstein, H.A., Feng, Y., Anderson, V.E., and Tonge, P.J. 1999. Role of glutamate 144 and glutamate 164 in the catalytic mechanism of enoyl-CoA hydratase. *Biochemistry* **38**, 9508–9516.

Holden, H.M., Benning, M.M., Haller, T., and Gerlt, J.A. 2001. The crotonase superfamily: divergently related enzymes that catalyze different reactions involving acyl coenzyme A thioesters. *Acc. Chem. Res*. **34**, 145–157.

Holm, L. 2019. Benchmarking fold detection by DaliLite v.5. *Bioinformatics* **35**, 5326–5327.

Hubbard, P.A., Yu, W., Schulz, H., and Kim, J.J. 2005. Domain swapping in the low-similarity isomerase/hydratase superfamily: the crystal structure of rat mitochondrial Delta3, Delta2-enoyl-CoA isomerase. *Protein Sci*. **14**, 1545–1555.

Kantardjieff, K.A. and Rupp, B. 2003. Matthews coefficient probabilities: Improved estimates for unit cell contents of proteins, DNA, and protein-nucleic acid complex crystals. *Protein Sci*. **12**, 1865–1871.

Kichise, T., Hisano, T., Takeda, K., and Miki, K. 2009. Crystal structure of phenylacetic acid degradation protein PaaG from *Thermus thermophilus* HB8. *Proteins* **76**, 779–786.

Kiema, T.R., Engel, C.K., Schmitz, W., Filppula, S.A., Wierenga, R.K., and Hiltunen, J.K. 1999. Mutagenic and enzymological studies of the hydratase and isomerase activities of 2-enoyl-CoA hydratase-1. *Biochemistry* **38**, 2991–2999.

Kim, E.J., Kim, Y.J., and Kim, K.J. 2014. Structural insights into substrate specificity of crotonase from the n-butanol producing bacterium *Clostridium acetobutylicum*. *Biochem. Biophys. Res. Commun*. **451**, 431–435.

Lee, D. and Kim, K.J. 2018. Structural insight into substrate specificity of 3-hydroxypropionyl-coenzyme A dehydratase from *Metallosphaera sedula*. *Sci. Rep*. **8**, 10692.

Matthews, B.W. 1968. Solvent content of protein crystals. *J. Mol. Biol*. **33**, 491–497.

Muller-Newen, G., Janssen, U., and Stoffel, W. 1995. Enoyl-CoA hydratase and isomerase form a superfamily with a common active-site glutamate residue. *Eur. J. Biochem*. **228**, 68–73.

Murshudov, G.N., Skubák, P., Lebedev, A.A., Pannu, N.S., Steiner, R.A., Nicholls, R.A., Winn, M.D., Long, F., and Vagin, A.A. 2011. REFMAC5 for the refinement of macromolecular crystal structures. *Acta Crystallogr. D Biol. Crystallogr*. **67**, 355–367.

Mursula, A.M., Hiltunen, J.K., and Wierenga, R.K. 2004. Structural studies on Δ(3)-Δ(2)-enoyl-CoA isomerase: the variable mode of assembly of the trimeric disks of the crotonase superfamily. *FEBS Lett*. **557**, 81–87.

Onwukwe, G.U., Koski, M.K., Pihko, P., Schmitz, W., and Wierenga, R.K. 2015. Structures of yeast peroxisomal Δ3,Δ2-enoyl-CoA isomerase complexed with acyl-CoA substrate analogues: the importance of hydrogen-bond networks for the reactivity of the catalytic base and the oxyanion hole. *Acta Crystallogr. D Biol. Crystallogr*. **71**, 2178–2191.

Otwinowski, Z. and Minor, W. 1997. Processing of X-ray diffraction data collected in oscillation mode. *Methods Enzymol*. **276**, 307–326.

Park, S.Y., Ha, S.C., and Kim, Y.G. 2017. The protein crystallography beamlines at the pohang light source II. *Biodesign* **5**, 30–34.

Partanen, S.T., Novikov, D.K., Popov, A.N., Mursula, A.M., Hiltunen, J.K., and Wierenga, R.K. 2004. The 1.3 A crystal structure of human mitochondrial Δ3-Δ2-enoyl-CoA isomerase shows a novel mode of binding for the fatty acyl group. *J. Mol. Biol*. **342**, 1197–1208.

Robert, X. and Gouet, P. 2014. Deciphering key features in protein structures with the new ENDscript server. *Nucleic Acids Res*. **42**, W320–W324.

Schuck, P. 2000. Size-distribution analysis of macromolecules by sedimentation velocity ultracentrifugation and lamm equation modeling. *Biophys. J*. **78**, 1606–1619.

Srivastava, S., Chaudhary, S., Thukral, L., Shi, C., Gupta, R.D., Gupta, R., Priyadarshan, K., Vats, A., Haque, A.S., Sankaranarayanan, R., *et al.* 2015. Unsaturated lipid assimilation by mycobacteria requires auxiliary *cis-trans* enoyl CoA isomerase. *Chem. Biol*. **22**, 1577–1587.

Tan, D., Crabb, W.M., Whitman, W.B., and Tong, L. 2013. Crystal structure of DmdD, a crotonase superfamily enzyme that catalyzes the hydration and hydrolysis of methylthioacryloyl-CoA. *PLoS One* **8**, e63870.

Thompson, J.D., Gibson, T.J., and Higgins, D.G. 2002. Multiple sequence alignment using ClustalW and ClustalX. *Curr Protoc Bioinformatics* Chapter 2, 2.3.1–2.3.22.

Vagin, A.A. and Teplyakov, A. 2010. Molecular replacement with MOLREP. *Acta Crystallogr. D Biol. Crystallogr*. **66**, 22–25.

van Weeghel, M., te Brinke, H., van Lenthe, H., Kulik, W., Minkler, P.E., Stoll, M.S., Sass, J.O., Janssen, U., Stoffel, W., Schwab, K.O., *et al.* 2012. Functional redundancy of mitochondrial enoyl-CoA isomerases in the oxidation of unsaturated fatty acids. *FASEB J*. **26**, 4316–4326.

Zhang, D., Yu, W., Geisbrecht, B.V., Gould, S.J., Sprecher, H., and Schulz, H. 2002. Functional characterization of Δ3, Δ2-enoyl-CoA isomerases from rat liver. *J. Biol. Chem*. **277**, 9127–9132.